Supporting Information

Parallel Multiphase Microflows: Fundamental Physics, Stabilization Methods and Its Applications

Authors:

Arata Aota[1,2], Kazuma Mawatari[1], Takehiko Kitamori[1,2,3]

Affiliations:

[1]Kanagawa Academy of Science and Technology

3-2-1 Sakado, Takatsu, Kawasaki, Kanagawa 213-0012, Japan.

Fax: +81-44-819-2092; Tel: +81-44-819-2037

[2] Institute of microchemical technology

3-2-1 Sakado, Takatsu, Kawasaki, Kanagawa 213-0012, Japan.

Fax: +81-44-811-6521; Tel: +81-44-811-5544

[3]The University of Tokyo

7-3-1 Hongo, Bunkyo, Tokyo 113-8656, Japan

Fax: +81-3-5841-6039; Tel: +81-3-5841-7231

Corresponding author contact information;

E-mail: kitamori@icl.t.u-tokyo.ac.jp

FLOW VELOCITY PROFILE OF PARALLEL TWO-PHASE MICROFLOWS

Phase I and II have viscosities of μ^{I} and μ^{II} and widths of a and b, respectively. As driving force of the flow, pressure difference of P_L-$P_o \equiv \Delta P$ is assumed for a channel length of L. The x- and z-axes are defined as directions across and along the channel, respectively. The origin of the x-axis is assumed at the interface of phases I and II. Under these conditions, shear stress τ_{xz} can be expressed based on momentum balance as,

$$\frac{d\tau_{xz}}{dx} = \frac{\Delta P}{L}. \qquad \text{(S1)}$$

In order to obtain the stress for phases I and II, integral calculus of Equation (S1) is expressed as

$$\begin{aligned} \tau_{xz}^{\mathrm{I}} &= \frac{\Delta P}{L} x + C_1^{\mathrm{I}} \\ \tau_{xz}^{\mathrm{II}} &= \frac{\Delta P}{L} x + C_1^{\mathrm{II}} \end{aligned}, \qquad \text{(S2)}$$

where C_1 is constant and superscripts I and II mean phases I and II. Here, continuity of shear stress is assumed as a boundary condition. Namely,

$$\tau_{xz}^{\mathrm{I}} = \tau_{xz}^{\mathrm{II}} \quad \text{at} \quad x = 0. \qquad \text{(S3)}$$

By substituting Equation (S2) with Equation (S3), the following relationship is obtained.

$$C_1^{\mathrm{I}} = C_1^{\mathrm{II}} = C_1. \quad \text{(S4)}$$

Here, Newton's law of viscosity is used,

$$\tau_{xz} = \mu \frac{dv_z}{dx} \tau_{xz}^{\mathrm{II}}, \quad \text{(S5)}$$

where v_z is flow velocity in the z-direction. By using Equations (S2), (S4) and (S5), the velocities of phases I and II, v^{I} and v^{II}, are expressed as

$$v_z^{\mathrm{I}} = \frac{\Delta P}{2L\mu^{\mathrm{I}}}x^2 + \frac{C_1}{\mu^{\mathrm{I}}} + C_2^{\mathrm{I}}$$
$$v_z^{\mathrm{II}} = \frac{\Delta P}{2L\mu^{\mathrm{II}}}x^2 + \frac{C_1}{\mu^{\mathrm{II}}} + C_2^{\mathrm{II}}, \qquad \text{(S6)}$$

where C_2 is a constant. Here, consistency of v_z^{I} and v_z^{II} at the interface and non-slip conditions are assumed as boundary conditions. Namely,

$$v_z^{\mathrm{I}} = v_z^{\mathrm{II}} \quad \text{at} \quad x = 0.$$

$$v_z^{\mathrm{I}} = 0 \quad \text{at} \quad x = a. \qquad . \quad \text{(S7)}$$

$$v_z^{\mathrm{II}} = 0 \quad \text{at} \quad x = -b.$$

From Equations (S6) and (S7), C_1, C_2^{I} and C_2^{II} are eliminated as

$$v_z^{\mathrm{I}} = \frac{\Delta P}{L}\frac{a^2}{\mu^I}\left[1 + \frac{\frac{b^2}{a^2}\mu^I - \mu^{II}}{\frac{b}{a}\mu^I + \mu^{II}} + \frac{\frac{b^2}{a^2}\mu^I - \mu^{II}}{\frac{b}{a}\mu^I + \mu^{II}}\left(\frac{x}{a}\right) - \left(\frac{x}{a}\right)^2\right], \quad \text{(S8)}$$

$$v_z^{\mathrm{II}} = \frac{\Delta P}{L}\frac{b^2}{\mu^{II}}\left[1 - \frac{\mu^I - \frac{a^2}{b^2}\mu^{II}}{\mu^I + \frac{b}{a}\mu^{II}} + \frac{\mu^I - \frac{a^2}{b^2}\mu^{II}}{\mu^I + \frac{b}{a}\mu^{II}}\left(\frac{x}{b}\right) - \left(\frac{x}{b}\right)^2\right], \quad \text{(S9)}$$

Figure S1 shows flow velocity profiles calculated based on Equation (S8) and (S9) for water (1.0 cP) -ethylacetate (0.43 cP) when the width of the phase I is equal to that of phase II, a=b.

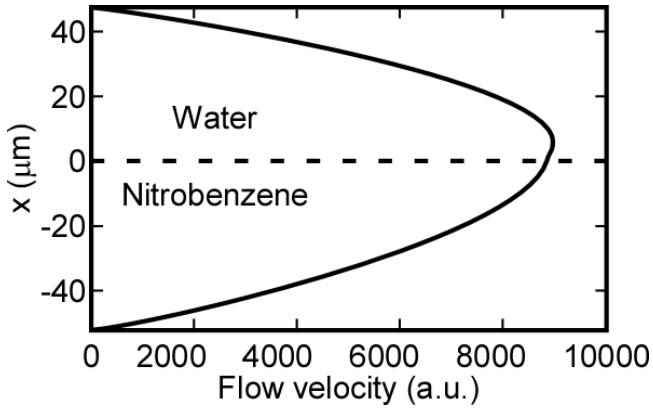

Fig. S1 Flow velocity profile of the water-nitrobenzene flow in a 100 μm-deep microchannel.

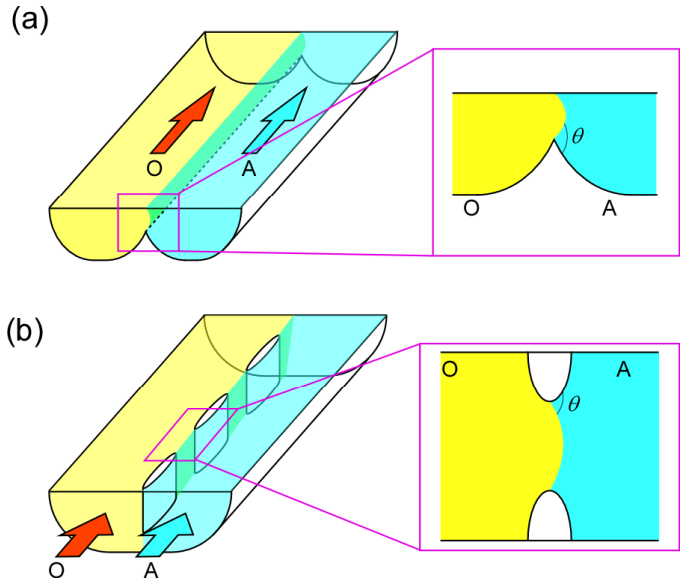

Fig. S2 Methods for the phase separation utilizing the microchannel structures. (a) Guide structure. (b) Pillar structure.

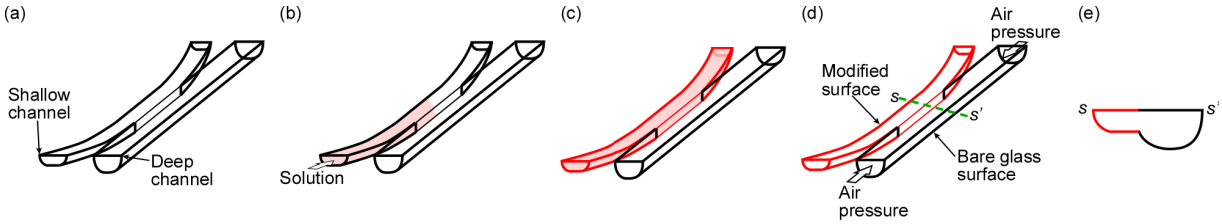

Fig. S3 Modification procedures by CARM method. (a) The shallow and deep microchannels have separate inlet holes and contact points in the microchip. (b) A solution containing modification compounds is introduced from the inlet of the shallow microchannel by capillarity. (c) The solution does not leak to the deep microchannel and only the shallow microchannel is modified. (d) The solution is pushed away with air pressure from the deep microchannel. (e) A sectional illustration along the s-s' dashed line in (d).

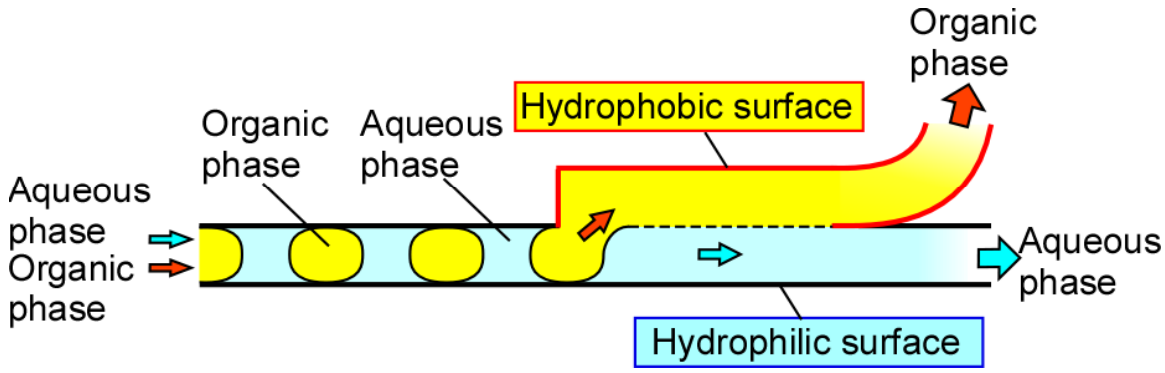

Fig. S4 Conversion of plug flow into parallel two phase microflows in the microchannel with the patterned surfaces.

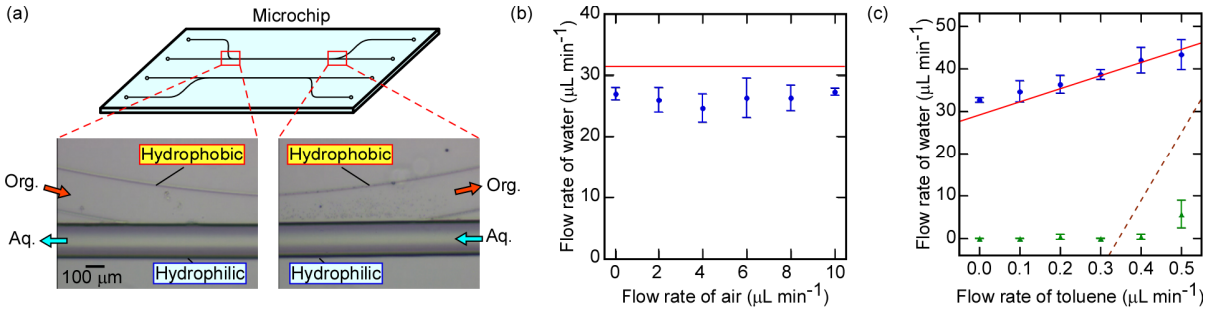

Fig. S5 (a) Optical microscope images of the phase separation at the confluences. (b) Maximum flow rate of water as a function of the flow rate of air. The *blue solid circles* show the experimental maximum flow rates, and the *red solid line* theoretical higher limit. (c) Maximum and flow rates of water as a function of the flow rate of toluene. The *blue solid circles* show the experimental maximum flow rates, the *green solid triangles* the experimental minimum flow rates, the *red solid line* theoretical higher limit, and the *brown dashed line* the theoretical lower limit.

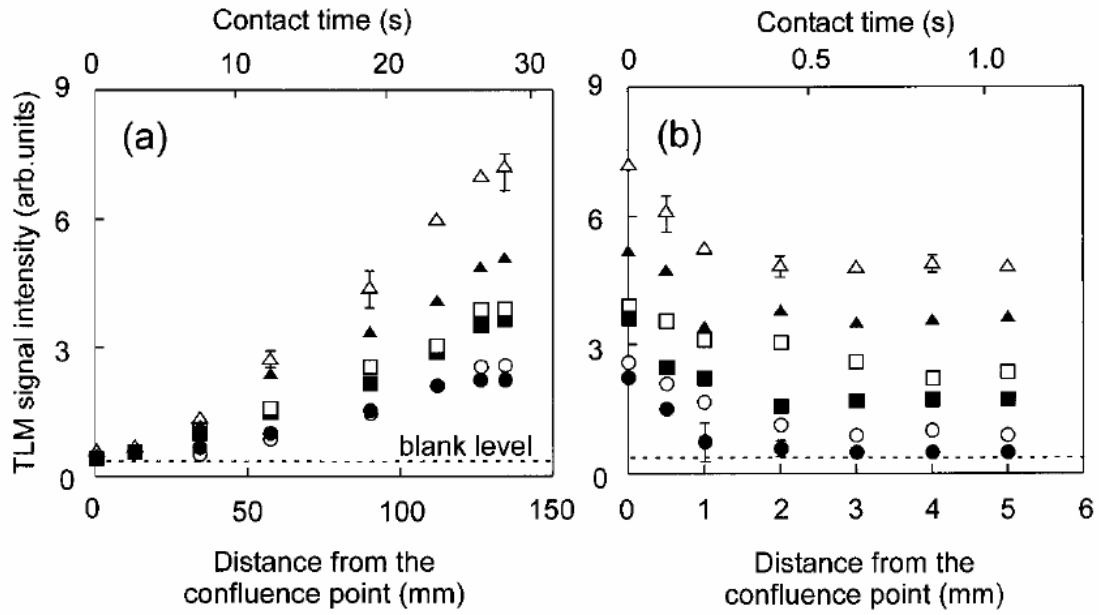

Fig. S6 Dependence of the TLM signal of the admixture sample on the distance from the confluence of (a) sample, reagent, and *m*-xylene and (b) HCl, *m*-xylene, and NaOH. The *open triangle*, *solid triangle*, *open square*, *solid square*, *open circle*, and *solid circle* correspond to 1.5×10^{-7}, 1.0×10^{-7}, 8.0×10^{-8}, 5.0×10^{-8}, 2.0×10^{-8}, and 0 M of Co(II). All samples included 1×10^{-6} M of Cu(II).

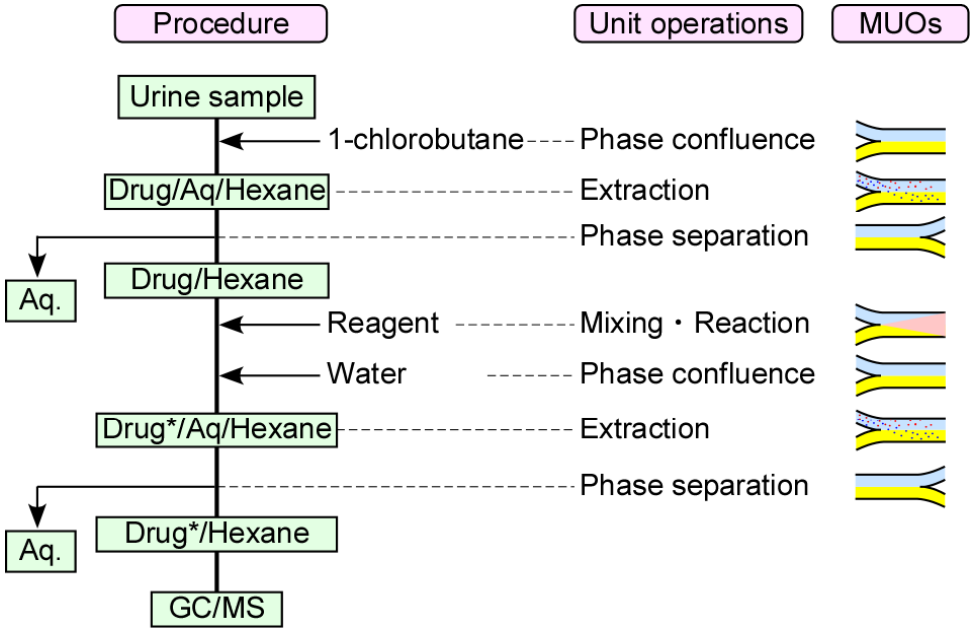

Fig. S7 Design of urine analysis systems based on MUOs and CFCP.

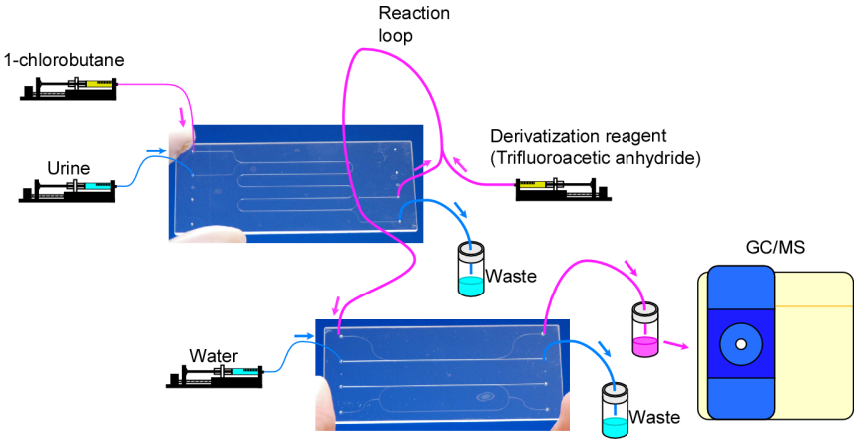

Fig. S8 Microsystems for urine analysis.